Accepted Manuscript

Precambrian plate tectonic setting of Africa from multidimensional discrimination diagrams

Sanjeet K. Verma

PII: S1464-343X(16)30350-8
DOI: 10.1016/j.jafrearsci.2016.11.001
Reference: AES 2714

To appear in: *Journal of African Earth Sciences*

Received Date: 10 May 2016
Revised Date: 25 October 2016
Accepted Date: 1 November 2016

Please cite this article as: Verma, S.K., Precambrian plate tectonic setting of Africa from multidimensional discrimination diagrams, *Journal of African Earth Sciences* (2016), doi: 10.1016/j.jafrearsci.2016.11.001.

Precambrian plate tectonic setting of Africa from multidimensional discrimination diagrams

Sanjeet K. Verma

División de Geociencias Aplicadas, Instituto Potosino de Investigación Científica y Tecnológica (IPICYT), Camino a la Presa San José 2055, San Luis Potosí 78216, Mexico

Corresponding Email: sanjeet.verma@ipicyt.edu.mx; sanjeet_vrm@yahoo.com

Manuscript Submitted to: **Journal of African Earth Sciences,** May 10, 2016, revised October 10, 2016, re-revised October 25, 2016.

ABSTRACT

New multi-dimensional discrimination diagrams have been used to identify plate tectonic setting of Precambrian terrains. For this work, nine sets of new discriminant-function based multi-dimensional discrimination diagrams were applied for thirteen case studies of Precambrian basic, intermediate and acid magmas from Africa to highlight the application of these diagrams and probability calculations. The applications of these diagrams indicated the following results: For northern Africa: to Wadi Ghadir ophiolite, Egypt indicated an arc setting for Neoproterozoic (746±19 Ma). For South Africa: Zandspruit greenstone and Bulai pluton showed a collision and a transitional continental arc to collision setting at about Mesoarchaean and Neoarchaean (3114±2.3 Ma and 2610-2577 Ma); Mesoproterozoic (1109±0.6 Ma and 1100 Ma) ages for Espungabera and Umkondo sills were consistent with an island arc setting. For eastern Africa, Iramba–Sekenke greenstone belt and Suguti area, Tanzania showed an arc setting for Neoarchaean (2742±27 Ma and 2755±1 Ma). Chila, Bulbul-Kenticha domain, and Werri area indicated a continental arc setting at about Neoproterozoic (800-789 Ma); For western Africa, Sangmelima region and Ebolowa area, southern Cameroon indicated a collision and continental arc setting, respectively for Neoarchaean (~2800-2900 Ma and 2687-2666 Ma); Finally, Paleoproterozoic (2232-2169 Ma) for Birimian supergroup, southern Ghana a continental arc setting; and Paleoproterozoic (2123-2108 Ma) for Katiola-Marabadiassa, Côte d'Ivoire a transitional continental arc to collision setting. Although there were some inconsistencies in the inferences, most cases showed consistent results of tectonic settings. These inconsistencies may be related to mixed ages, magma mixing, crustal contamination, degree of mantle melting, and mantle versus crustal origin.

Keywords: Africa continent, tectonic setting, Precambrian rocks, log-ratio transformation, geochemistry, probability calculations

1. Introduction

The origin of the Precambrian terranes is full of uncertainties, which is due to their geological and geochronological complexity. In context of plate tectonic setting, the Precambrian is one of the most controversial era and questions still remain of what was Earth´s tectonic style during the Precambrian. To answer the question such as whether plate tectonic operates in the Neoarchaean, several multidisciplinary studies (geochemical, geophysical, geochrological and petrological data as well as numerical modelling) have been published (e.g., Ernst 2009; Van Kranendonk 2010; Korsch et al., 2011). Some researchers (e.g., Stern 2008; Hamilton 2011) believed that this may be possible for the Proterozoic. Despite the large data base available, researchers still disagree on plate tectonic setting during the Precambrian (e.g., Foley 2008; Pease et al., 2008; Shirey et al., 2008; Furnes et al., 2009). The Precambrian terranes in Africa are diverse, including a number of Archaean cratons such as west African Craton, Congo Craton, Tanzania Craton, Kaapvaal Craton and numerous Paleoproterozoic, Mesoproterozoic, and Neoproterozoic mobile belts. The major part of the earth history about geological records preserve in these cratonic bodies and related to continental break-up and growth which have been recognized worldwide and can be largely explained in a complicated plate tectonic context (Goodwin, 1996; Torsvik et al., 2009). Therefore, very first question of African geology specially related to Precambrian tectonic setting is still unanswered and debatable. This continuing debate encourages us to make an attempt to apply new robust techniques, i.e., multi–dimensional discrimination diagrams to explore plate tectonic setting for such Precambrian terrane (e.g., igneous and meta-igneous rocks) of the African continent.

For this work, nine sets (a total of forty-five) new mutli-dimensional discrimination diagrams have been used which is based on linear discriminant analysis (LDA) of log-transformed ratios of all major elements and selected relatively immobile major and trace elements. These diagrams are based on basic (Verma et al., 2006; Verma and Agrawal, 2011), intermediate (Verma and Verma, 2013) and acid (Verma et al., 2012; 2013) magmas. The traditional tectonomagmatic discrimination diagrams such as bivariate and ternary proposed by several researchers (e.g., Pearce and Cann, 1973; Pearce and Gale, 1977; Pearce and Norry, 1979; Wood 1980; Pearce 1982; Shervais 1982; Meschede 1986; Cabanis and Lecolle, 1989), are well known and highly used by the researchers all over the world. The principle advantage of ternary diagrams indicates visualizing capacity in two dimension of the three variables in two dimensions. Further, the relative proportions of the ternary variables are clearly visible in the diagram, although this should be equally clear from the three measured concentration values themselves. The main disadvantage of using measured crude compositions or those adjusted to 100% in binary and ternary diagrams is that they violate the basic assumption of randomness and normal distribution of the plotted variables (Verma 2015a). Verma (2010) evaluated all traditional diagrams and showed that none of them are functioning better because most of them provided unacceptably low success rates and allowed the discrimination of only a limited number of plate tectonic settings. Their major defects, viz., use of limited databases, problem of closed or constant sum compositional variables, and eye-fitted tectonic field boundaries, were prevalent in all of them (Agrawal and Verma, 2007). Therefore, advance of new multi-dimensional diagrams could be a better option for accuracy and correct discrimination.

Out of nine sets (two sets for basic diagrams (Verma et al., 2006; Verma and Agrawal 2011), three sets of the five diagrams each for intermediate magma (Verma and Verma, 2013) and four sets of five each for acid magma (Verma et al., 2012, 2013) have also been recently available for the discrimination of four tectonic settings (island arc, continental arc, within-plate, and continental collision). These sets involve coherent statistical treatment of compositional data consisting of log-ratio transformation, being a fundamental requirement for such data handling (Aitchison 1986; Egozcue et al., 2003; Pawlowsky-Glahn and Egozcue, 2006; Buccianti 2013; Verma, 2015). Further, basic, intermediate and acid diagrams (Verma et al., 2006; Verma and Agrawal 2011; Verma and Verma, 2013; Verma et al., 2012, 2013) are based on log-ratios of either all major elements [$(SiO_2)_{adj}$, $(TiO_2)_{adj}$, $(Al_2O_3)_{adj}$, $(FeO)_{adj}$, $(Fe_2O_3)_{adj}$, $(MnO)_{adj}$, $(MgO)_{adj}$, $(CaO)_{adj}$, $(Na_2O_3)_{adj}$, $(K_2O)_{adj}$, $(P_2O_5)_{adj}$] a combination of selected relatively immobile major and trace elements [$(TiO_2)_{adj}$, $(MgO)_{adj}$, $(P_2O_5)_{adj}$, Nb, Ni, V, Y, and Zr), or only selected relatively immobile trace elements (La, Ce, Sm, Yb, Nb, Th, Y, and Zr).

These diagrams have successfully applied several case studies world-wide. For Africa (south Africa and northern Cameroon, e.g., Bailie et al., 2010, 2012; Bouyo et al., 2016 confirmed an arc setting by using these diagrams for Archaean and Neoproterozoic basic and acid rocks); For Brazil (Amazonian, São Francisco, São Luís craton, and Borborema province, e.g., Verma and Oliveira 2013, 2015; Verma et al. 2015a, 2015b; Cioffi et al., 2016 used these multidimensional diagrams to infer tectonic setting of Archaean to Proterozoic basic to acid rocks); For India (Dharwar and Bundelkhand craton, e.g., Verma et al. 2015a; Bora and Kumar, 2015; Kaur et al., 2015 have successfully applied these diagrams for Archaean basic to acid rocks); For China (North China Craton and Jitang complex in Leiwuqi area, e.g., Verma et al. 2015a; Hu et al., 2014 were used these discrimination diagrams for Archaean and Paleozoic basic to acid rocks); For Australia (Lachlan Orogen, southeast Australia, central Australia, e.g., Medlin et al., 2015; Offler and Fergusson, 2016 used these diagrams for Palaeozoic acid rocks); For Russia, Italy and Iran e.g., Grebennikov (2014) has suggested to use these diagrams for granites and related rocks; Perri et al., 2015; Yildiz et al., 2015 and Shahzeidi et al., 2006 also applied these diagrams for Neoproterozoic to Holocene basic to acid rocks. For Mexico-Argentina (Mexican Volcanic belt, Oaxaca, Granjeno Schist, San Nicolás and San Carlos and Gulf of Mexico), researchers (Verma 2009, 2013; 2015; Verma et al., 2011, Armstrong-Altrin et al., 2014; Pandarinath 2014a, 2014b; Pandarinath and Verma 2013, Velasco-Tapia, 2014; Armstrong-Altrin, 2015; Torres Sánchez et al., 2015; Verma et al., 2016a) have applied these diagrams for Cenozoic to Neoproterozoic basic to acid rocks). Other researchers (Velikoslavinskii and Krylov, 2015; Zhou, 2015; Rossignol et al., 2016; Janoušek et al., 2016) have been also used these diagrams.

In this work, these multi-dimensional geochemical discrimination diagrams (two sets of basic diagrams i.e., major and immobile trace elements by Verma et al., 2006; Verma and Agrawal, 2011; three sets of intermediate diagrams i.e., major elements, major-trace elements and immobile trace elements by Verma and Verma 2013; and four sets of acid diagrams i.e., two sets of major elements, one major-trace elements and one immobile trace elements based diagrams by Verma et al., 2012, 2013) were used to identify plate tectonic setting of Precambrian intermediate and acid rocks from Africa.

2. Multidimensional tectonomagmatic diagrams and their application

These diagrams are based on the techniques log-ratio transformation and linear discriminant analysis (LDA) and canonical analysis. Probability values for individual samples were calculated from the method outlined by Agrawal (1999) and Verma and Agrawal (2011) and used in this work to decide the discrimination tectonic field in which a given sample will plot. The discriminant functions (DF1-DF2) for these diagrams were calculated from equations. Although a computer program which can be obtained from website http://tlaloc.ier.unam.mx/index.html that facilitate the use of these complex equations. Nevertheless, these equations are also summarized in Supplementary Material file Tables S1–S6. These diagrams are required to discriminate five tectonic settings of Island arc (IA), continental arc (CA), continental rift (CR), ocean-island (OI) and collision (Col). For each diagram, two functions must be calculated for each compiled sample (Verma 2012; Verma and Verma 2013, Verma et al., 2012, 2015, 2016).

3. Construction of data base

The data base was compiled from published literature of Precambrian rocks (Table 1). This include serval localities: **North Africa** (Wadi Ghadir ophiolite, Egypt–Abd El-Rahman et al., 2009); **South Africa** (Zandspruit greenstone–Anhaeusser, 2015; Bulai pluton–Laurent et al., 2011; Espungabera – Moabi et al., 2015; Umkondo LIP–Bullen et al., 2012). **East Africa** (Iramba-Sekenke greenstone belt, central Tanzania–Manya and Maboko, 2008; Suguti area, northern Tanzania–Mtoro et al., 2009; Chila and Werri, northern Ethiopia–Tadesse-Alemu, 1998; Bulbul-Kenticha domain, southern Ethiopia–Yihunie et al., 2006; and Sifeta et al., 2005). **West Africa** (Sangmelima region and Ebolowa area, southern Cameroon– Sang et al., 2004 and Tchameni et al., 2000; Birimian supergroup, southern Ghana–Grenholm, 2011, Anum et al., 2015; Katiola-Marabadiassa, Côte d'Ivoire–Doumbia et al., 1998).

A synthesis of the relevant information (locality, approximate location, number of compiled samples, age, original Author´s tectonic setting, inferred tectonic setting, and literature references) is provided in Table 1. A schematic map showing the location of the studied area is provided in Figure 1. Detailed geology and locations of samples can be consulted in the papers from which the data were compiled.

IgRoCS (Verma and Rivera-Gómez, 2013) computer program was used for the classification of magma types according to the IUGS criteria, whereas TecDIA (Verma et al., 2016b) was used to deciphering plate tectonic setting and probabilities calculation of each plotted samples for intermediate and acid magmas (Verma and Verma, 2013; Verma et al., 2012, 2013).

4. Result and Discussion

The data from the above localities were plotted in the corresponding multidimensional diagram (Figs. 2, S1–S6). The results are summarized in Tables 2–4, S7–S32, with percentage probabilities calculations. Each tectonic setting (IA=Island Arc; CA=Continental Arc CR=Continental Rift; OI=Ocean Island; and Col=Collision) were identified based on total percentages probabilities (Tables 2–4, S7–S32). Further, Tables 2–4, S7–S32 includes % percentage probability estimates and synthesis of the number of samples plotting in each diagram (Figs. 2, S1–S6) from the %probability values. Thus these plots (Figs. 2, S1–S6) are for reference purpose only because %probability values estimates (Tables 2–4, S7–S32) are fully understandable without considering the plots.

Northern Africa

1. Wadi Ghadir ophiolite, Eastern Desert, Egypt

The Neoproterozoic ophiolites of Wadi Ghadir area is located in the central part of the Eastern Desert of Egypt (Abd El-Rahman et al., 2009). This rock is mainly composed of gabbroic (ophiolitic) in nature and containing pyroxene, plagioclase, and pegmatitic minerals. According to original authors (Abd El-Rahman et al., 2009), the MORB normalized trace element indicates subduction related environment due to negative Nb and Ta anomalies. Further, Abd El-Rahman et al., 2009 concluded that such geochemical characteristics are consistent with magma compositions generated in supra-subduction zone settings.

For better understanding, the first case study will be explored and expanding with detail explanation. For this area of Wadi Ghadir ophiolite, thirty-four, fifty and two samples of Neoproterozoic basic, intermediate and acid rocks respectively (protolith age of 746±19 Ma; Abd El-Rahman et al., 2009) showed an arc setting. Two sets of diagrams (m2 and t2, Verma et. al., 2006; Verma and Agrawal, 2011, Table 1) based on log-ratios of major elements and immobile trace elements indicated arc to mid-ocean ridge setting with total percentage probability values of about 33% and 59%, respectively (Table 2).

For intermediate volcanic rocks (fifty samples with complete major elements, immobile major and trace elements and trace elements were available; see values for M, MT, and T for test study 1 in Table 1), all three sets of diagrams (Verma and Verma, 2013) could be applied for this case study, which clearly indicated an arc setting. The first set of diagrams which is based on major elements showed a continental arc (CA) setting with total percent probability values of about 38%, while other two sets i.e., based on immobile major-trace and trace elements indicated an island arc setting with total percent probability values of about 41% and 58% respectively (Table 3, Figs. 2 and S1-S2).

Only two samples of acid rocks had complete data for major elements, immobile major and trace elements and immobile trace elements (Table 4). All sets based on log-ratios of major elements, immobile major and trace elements, and immobile trace elements (Verma et al., 2012, 2013; Table 3) provided clear cut answer of an island arc setting for this area, with high total percent probability values of about 75%, 75%, 73%, and 75%, respectively (Table 4, S3–S6).

This finding is consistent with original authors (Abd El-Rahman et al., 2009) interpretation of subduction related environments.

South Africa

2. Zandspruit greenstone, Johannesburg dome

The Johannesburg dome consists of granitic rocks, gneisses and greenstones (komatiites) in the central part of the Kaapvaal Craton, South Africa. The Zandspruit greenstone is situated in the west-central part of this dome. This sector is covered by porphyritic phase of the granodiorites having zircon age of 3114 ± 2.3 Ma (Poujol and Anhaeusser, 2001). The rocks from this area are medium- to coarse-grained with quartz, K-feldspar, plagioclase, and biotite, also with accessory minerals, i.e., comprising of zircon, apatite, etc.

For Mesoarchaean (3114 ± 2.3 Ma) Zandspruit greenstone, (Anhaeusser, 2015), only two sets could be applied for basic rocks (Verma et al., 2006; Verma and Agrawal, 2011, Table 1), these diagrams showed an island arc setting with total percentage probability values of about 80% and 80%, respectively (Table S7).

Two sets of intermediate rock which is based on log-ratios of major elements and immobile major elements indicated a collision setting with total percent probability values of 74% and 61%, respectively, (Table S7, Figs. 2 and S1). Nine samples of acid rock indicated a collision setting in the diagrams based on log-ratios of major elements (total percent probability values of 70% and 72%, (Table S8, Figs. S3–S4). The second sets major-trace elements based diagrams also indicates collision setting with (total percent probability values of 80%, Table S8, Figs. 2 and S1). In summary, all sets of diagrams (Verma and Verma, 2013; Verma et al., 2012, 2013) showed collision setting.

Although, Anhaeusser, 2015 did not comment on tectonic setting. Nevertheless. New multi-dimensional diagrams showed an arc-collision setting.

3. Bulai pluton, Central Limpopo Belt

The Bulai pluton is a magmatic body of the Central zone of the Limpopo Belt (Limpopo Province, South Africa). This pluton is covered by porphyritic granodiorite having different mineral assemblage like K-feldspar, plagioclase, hornblende and biotite. The zircon yield pluton-emplacement ages ranging between 2.58 and 2.61 Ga (Laurent et al., 2011).

For this application (Neoarchaean, about 2610-2577 Ma; Laurent et al., 2011), eleven samples of intermediate rocks with major, major-trace and trace elements data were available (Table

1). All three sets indicated collision setting with total percent probability values of 63%, 79% and 83%, respectively (Table S9, Figs. 2, S1–S2). Fourteen samples of acid rocks were available for the application, two sets of diagrams based on log-ratios of major elements and one set on immobile major-trace elements indicated a collision setting with total percent probability values of 79%, 75 and 74%, respectively (Table S10, Figs. S3–S5), whereas the third set based on log-ratios of immobile trace elements was more consistent with a continental arc setting (total percent probability of 59%; Table S10, Fig. S6).

The results suggest that these rocks are more consistent with a collision setting, or a transitional continental arc to collision setting for the Bulai pluton. According to (Holzer et al., 1998; Roering et al., 1992), the Limpopo belt corresponds to a complex Himalayan-type orogenic belt but they did not explain about the tectonic setting. Laurent et al. (2013) suggested a possible late orogenic setting for the generation of the Bullai pluton.

4. Espungabera, Mozambique

The Espungabera volcanic formation is situated in central Mozambique which correlates with the Umkondo sills in eastern Zimbabwe. The rocks are mainly two types 1) volcanic outcrops which are 15-20 m in height and 2) basaltic andesite of 3 m in diameter. The thin section reveals euhedral plagioclase phenocrysts with sausseritic alteration hosted in an aphanitic matrix. Besides plagioclase, other mineral like otho- and clinopyroxene are present.

According to Moabi et al. (2015), The Umkondo tholeiitic is coetaneous with tonalitic calc-alkaline of the Nampula and Maud Terranes in Mozambique which is also similar with the Kalahari Craton. This finding indicates that the Espungabera volcanic formation is the part of a back-arc setting, or volcanic arc/subduction related environment along with the eastern margin of Kalahari Craton.

For this application to Mesoproterozoic (1109±0.6) basaltic andesite rocks from the Espungabera, Mozambique region (Moabi et al., 2015), three sets of intermediate diagrams were applied. The all sets of diagrams indicated an island arc (IA) setting, with relatively higher percentage of 70, 78% and 59%, respectively (Table S1, Figs. 2, S1–S2. Thus, from intermediate rocks, an island arc setting can be inferred for the Espungabera volcanic formation. This result is also somehow consistent with original author (Moabi et al., 2015) finding. For tectonic discrimination they used Zr–Nb–Y tectono-classification diagram of Meschede (1986), and mostly samples were plotted in combined filed of within-plate and volcanic arc setting which is unclear answer of exact tectonic setting. The application of new multidimensional diagrams provide a clear cut answer of arc related environment.

5. Umkondo sills (Waterberg, Middelburg) Kalahari craton

The Umkondo sills were emplaced into continental crust of the Kalahari craton. Further, these sills are most extensively developed in the Waterberg and Middelburg basins in northern South Africa and south-eastern Botswana. The Waterberg basin is further renamed as Mesoproterozoic Post-Waterberg sills A (MPWA sills), only small number of samples were recognised as (MPWB sills) for Middelburg basins. The samples from the area (MPWA sills) are dolerites, gabbros and noritic gabbros, having mineral composition of augite, labradorite, and magnetite, whereas MPWB sills are dolerites and gabbros, having augite, labradorite and magnetite mineral. For this application, the data base was compiled from these areas i.e., MPWA, MPWB and Botswana. According to Bullen et al. (2012), the samples for MPWA sills were characteristically LREE enriched with relatively unfractionated HREEs, and the normalised incompatible element similar to modern island arc andesites.

Two sets of diagrams based on log-ratios of major elements and immobile major and trace elements indicated an island arc setting with total percentage probability values of about 44% and 80% (Table S13), respectively. All three sets of diagrams indicated an island arc (IA) setting for intermediate rocks from this area during the Mesoproterozoic (1100 Ma; Bullen et al., 2012; Table S14), the total percent probability values were 72%, 66% and 57%, respectively (Table S14, Figs. 2, S1–S2). Unfortunately, no acid rock sample was available for this application.

The authors (Bullen et al. 2012) explained that primitive mantle-normalised spider diagrams for MPWA samples indicated modern type island arc setting or subduction related environment which is also supported by petrogenetical studies. The application of new multi-dimensional diagrams also showed an island arc (IA) setting for MPWA, MPWB area which is also consistent with interpretation of Bullen et al. (2012).

Eastern Africa

6. Iramba-Sekenke greenstone belt, central Tanzania

The Iramba–Sekenke greenstone belt is located in central part of the Tanzania Craton. the oldest rocks in the area are the granite-gneisses found in the north and northeast of the belt. Manya and Maboko (2008) investigated about volcanic rocks which is also constitute of this greenstone belt. The volcanic rocks consist of several mineral components like rare olivine, pyroxenes, plagioclase, quartz, amphibole. On primitive normalization diagram the large number of samples showed negative anomalies of Nb, Ta and Ti, which reveals that formation of these rocks are in back-arc setting.

The Neoarchaean (2742±27 Ma) basic and intermediate rocks from this area showed an island arc setting with total percent probability of 77% and 80% for basic rocks and 51%, 40% and 58%, respectively for intermediate rocks (Table S15–S16, Figs. 2, S1–S3)

Manya and Maboko (2008) used several discrimination diagrams of (Pearce and Cann, 1973; Wood, 1980) to infer an island arc or back-arc setting for their intermediate rock samples. The result from new multi-dimensional showed an island arc setting for basic and intermediate rock samples, this result somehow supports the finding of original authors (Manya and Maboko, 2008)

7. Suguti area, northern Tanzania

The Suguti area is located in the north-eastern part of the Neoarchaean granite-greenstone terrane of the Tanzania Craton. The rocks from this area is mainly composed of tholeiitic basalts, andesites and calc-alkaline rhyolites and amount of intermediate rocks.

For Neoarchaean volcanic rocks (basaltic andesite and rhyolite) from Suguti area (2755±1 Ma; (Table 1) were compiled from the paper published by the Mtoro et al. (2009). 20 basic rock samples were available (Table 1). One set of major-element-based and one set of immobile-element ratio- based diagrams showed an island arc setting (Table S17).

For twelve samples of intermediate rocks the diagrams based on log-ratios of major elements, immobile major and trace elements, and trace elements indicated an island arc setting with total percent probability of 66%, 61% and 69% respectively (Table S18, Figs. 2, S1–S2). The second set of diagrams based on log-ratios of immobile major and trace elements also suggested an island arc setting but with less total percent probability of 45%. The third set of diagrams was more consistent with a collision setting.

For more numerous (twenty-five) acid rock samples, two sets of diagrams (log-ratios of major elements and of major and trace elements) indicated a collision setting with total percent probability values of 63% and 39% (Table S19, Figs. S3–S6). The second set based on major-trace element ratios, was more consistent with a within-plate transitional setting (probability values of 66%), whereas the one based on immobile trace element ratios indicated a continental arc setting with relatively low total percent probability of 45% (Table S19, S6). Therefore, discrimination diagrams based on acid rocks did not provide a clear cut answer for tectonic setting of Suguti area, whereas intermediate rocks were indicated an island arc setting for this area.

The original authors (Mtroro et al., 2009) used Ti–Zr–Y and Ti–V diagrams of Pearce and Cann (1973) and Shervais (1982) to discriminate tectonic setting. All diagrams showed an arc setting the Suguti area, which is consistent with result of new multidimensional diagrams for intermediate rocks.

8. Chila, Axum area, northern Ethiopia

Chila is situated in the Axum area of northern Ethiopia. The Chila rocks are mainly granitoids of Neoproterozoic age. The granitoids are essentially composed of plagioclase, quartz, biotite, hornblende, epidote, K-feldspar, sphene, and traces of apatite and zircon. These granitoids are enriched in incompatible elements. Further the depleted REE patterns of Nb and Ti indicate arc/or island-arc environment for these granitoids.

For this area, ten and forty-one samples could be compiled for intermediate and acid rocks, respectively; Table 1. Only two sets of intermediate diagrams were applied due to incomplete elements for trace element based diagrams. Both sets of intermediate diagrams indicated continental arc (CA) setting with percent probability values of 43% and 55%, respectively (Table S20, Figs. 2 and S1. However, forty-one samples (Table 1) were available for Neoproterozoic acid rocks (about 800 Ma; Tadesse-Alemu, 1998) from chila. These samples also indicated continental arc (CA) setting (with total percent probability values for CA tectonic settings in three sets of diagrams were 60%, 50% and 76%; fourth set of trace elements could not apply due to incomplete trace elements, Table S21, Figs. S3–S5).

Tadesse-Alemu (1998) postulated that the Chila granitoids constitute arc systems. He used (Y+Nb)-Rb discrimination of Pearce et al. (1984) and indicated a volcanic arc setting. The results of new multidimensional discrimination diagrams are also consistent with a continental arc (CA).

9. Bulbul-Kenticha domain, Negele area, northern Ethiopia

The Bulbul domain is composed of greenschist to lower amphibolite facies semi-pelitic and carbonaceous sediments, marble, amphibolite, mafic-ultramafic schists and serpentinite, whereas kenticha domain consist of amphibole schist, metabasalt, semi-pelitic, ultramafic and epidotized mafic schists. Yihunie et al. (2006) explained that the chemical characteristics of Bulbul-Kenticha domains are similar to back-arc basin and island-arc environment.

One set of major elements based diagram (Verma et al., 2006, Table 1) showed an island arc setting with percent probability of 42% (Table S22). The diagrams for basic magmas (Verma et al. 2006; Verma and Agrawal 2011) cannot discriminate the island arc from the continental arc setting. The two sets of intermediate diagrams were applied for this application. The diagrams based on log-ratio of major elements showed continental arc setting (the total probability value of 47%, Table S23, Figs. 2, S1), whereas the immobile trace elements diagrams indicated an island arc setting with total percent probability of 39% (Table S23, Figs. 2, S2).

The original authors have applied ternary diagram of (Pearce and Cann, 1973), the most of samples were plotted on the ocean floor basalt field with some plot on the island-arc and within plate basalt fields. Further, they suggested that suggesting that the Negele metabasic rocks were formed at back-arc and island-arc tectonic environments. New multidimensional diagrams showed an arc setting for this area.

10. Werri area, northern Ethiopia

Werri area consist of Neoproterozoic metavolcanic and metasedimentary rocks which are wide spread in northern Ethiopia. The metavolcanic rocks were only complied for the application. These rocks contain coarse phenocrysts of plagioclase and altered mineral viz. calcite, chlorite, sericite, epidote, and fine-grained plagioclase. The age of the Werri metavolcanic rocks is not known. However, other metavolcanic rock sequences around the Werri area are intruded by post-tectonic granites with a Rb–Sr errorchron age of 550 Ma (Tadesse et al., 2000). On the basis of trace element geochemistry and chondrite-normalized REE patterns, Sifeta et al. (2005) suggested that these metavolcanic rocks are tectonically interpreted as volcanic arc setting.

For this Neoproterozoic (Sifeta et al., 2005; Table 1) Werri area, basic and intermediate rocks were available for application, the set of diagrams based on log-ratios of trace elements (Verma et al., 2006) indicated an island arc setting whereas (Verma and Agrawal, 2011) diagrams showed a transitional (arc to mid-ocean ridge) tectonic setting with percent probability of 70% and 80%, respectively (Table S24). All three sets of diagrams for intermediate rocks based on log-ratios of major, immobile major-trace and trace elements indicated a continental arc setting, with total percent probability values of about 64%, 68% and 69%, respectively (Table S25, Figs. 2, S1–S2). Sifeta et al. (2005) used several conventional bivariate and ternary diagrams (Shervais 1982; Pearce and Cann, 1973; Wood. 1980) to infer the tectonic setting. They hypothesized an arc or overlap of MORB setting for their samples. The new multidimensional study indicates a continental arc tectonic setting, which may be consistent with Sifeta et al. (2005). This is an advantage of new multi-dimensional diagrams to avoid overlap field.

Western Africa

11a. Sangmelima region, Ntem complex, southern Cameroon

Sangmelima region (Ntem complex, Congo craton) is composed of tonalite-trondhjemite-granodiorite (TTG) and charnockitic suite. These rocks have mineral composition of plagioclase, bluish quartz, feldspars, amphibole and biotite. According to Shang et al. (2004) the primitive mantle normalised spidergrams showed negative Nb–Ta anomalies, which suggested a subduction related setting for this area.

For this application to Neoarchaean (~2687-2666 Ma, Shang et al., 2004) rocks, two sets of intermediate diagrams were showed continental arc setting with total percent probability value of 46% and 53% (Table 26, Figs. 2, S1) whereas third set based on immobile trace elements indicated a collision setting with percent probability value of 43% (Table 26, Figs. 2, S2). For acid rock all sets of diagrams indicated a continental arc setting except first set of major-elements based diagrams more consistent with island arc setting with total percent probability value of 60%, 52% and 62%, respectively (Table 27, Figs. S3–S6). In totality, three sets of diagrams were consistent with continental arc.

Thus, all sets of diagrams showed an answer of island arc to continental arc setting for Sangmelima region, which is also consistent with the original author´s finding.

11b. Ebolowa area, Ntem complex, southern Cameroon

The Ebolowa area of (Ntem Complex, Congo Craton) consist of the Neoarchaean granitoids which is situated in southern Cameroon and contain xenoliths of the tonalite-trondhjemite-granodiorite (TTG) having principal mineral of plagioclase, amphibole, quartz and biotite.

Three sets of diagrams for eleven samples of Neoarchaean intermediate rocks (2687–2666) Ma granitoids; Tchameni et al., 2000) indicated a collision setting, with relatively high total percent probability values of 69%, 69%, and 54% respectively (Table S28, Figs. 2, S1–S2). The original authors (Tchameni et al., 2000) did not comment on the tectonic setting for their samples.

12. Birimian supergroup, southern Ghana

Birimian supergroup, southern Ghana comprises a part of the West African craton which consists of greenstone belts of volcanic and sedimentary rocks. In this belt, two generations of granitoids were intruded and emplaced in a subduction setting between 2232-2169 Ma

(Grenholm, 2011; Anum et al., 2015). The granitoids have several mineral compositions of biotite, hornblende, quartz, K-feldspar and plagioclase.

Only one set of major elements based diagram (Verma et al., 2006) showed an island arc setting with total percent probability of 54% (Table S29). One set of diagram indicated a collision setting for intermediate rocks from this area during the Paleoproterozoic (2232-2169 Ma; Grenholm, 2005; Anum et al., 2015; Table S30), whereas the set based on log-ratios of immobile major-trace elements showed a continental arc setting (with total percent probability value of 53% and 51 % respectively, Table S30, Figs. 2, S1). A continental arc setting was also indicated by all four sets of diagrams (log-ratios of major elements and immobile major and trace elements; Verma et al., 2012, 2013) for acid rocks (Table S31). The all sets of diagrams provided coherent result; the total percent probability values were (43%-65%) for three tectonic settings (Table S31, Figs. S3–S6).

The authors (Grenholm, 2011; Anum et al. 2015) were used (Rb-Y+Nb), (Nb-Y), (Rb-Ta+Yb) and (Ta –Yb) discrimination diagrams of Pearce et al. (1984) for acid rocks, most of samples were plotted in the field of volcanic arc granites. Thus, these authors suggested an arc or subduction related setting for this area. Also a continental arc setting is indicated from the application of new multi-dimensional diagrams.

13. Katiola- Marabadiassa, Côte d'Ivoire

Kaliola Marabadiassa granitoids consist of two generations lithostratigraphic data: the first generation intruding the greenstone formations (Timb and Tafolo, Kanangono, Fronan and N'Guessankro) and the second generation intruding the Bandama sedimentary basin formations and/or the earlier granitoid intrusions. For this application, only first generation geochemical data for granitoids were used, which has Paleoproterozoic age of (2123-2108 Ma). According to Ledru et al. (1994) and Feybesse and Mildsi (1994), the modern plate tectonics setting for this area is consistent with collision setting.

Forty-eight samples of acid rock samples (Kaliola Marabadiassa granitoids) of about 2123-2108 Ma (Paleoproterozoic; Doumbia et al., 1998; Table 1) were plotted in four sets of multi-dimensional diagrams. Two sets of major-elements based diagrams were indicated a collision setting with total percent probability value of 39% and 42% (Table S32, Figs. S3–S4) whereas major-trace elements and trace elements diagrams were indicated an island and continental arc setting, respectively, with total percent probability value of 50% and 57% (Table S32, Figs. S5–S6).

Although the original authors (Doumbia et al., 1998) did not comments on tectonic setting. The new multidimensional diagrams indicate an arc to collision transitional setting for this area.

5. Limitation of multidimensional discrimination diagrams

Although, the limitation of these diagrams have been already described in detail by Verma et al. (2015a), nevertheless, a brief discussion could be seen here i.e. related to the geochemically analyzed samples, data quality– precision and, more importantly, accuracy – of the analytical results, scarcity of large number of data base, radiometric ages. Other difficulties may be related to mixed ages, magma mixing, crustal contamination, degree of mantle melting, and mantle versus crustal origin. The crustal contamination and crustal versus mantle origin were fully elaborated and illustrated in the papers on the Neogene-Quaternary Mexican Volcanic Belt (MVB; for example, for the eastern and central MVB by Verma 2015b, 2015c, and for the western MVB by Verma et al., 2016a). Further, MVB acid rocks showed the tectonic setting of the crustal source rocks that may have formed earlier in a tectonic setting different from the actual tectonic setting of the basic and intermediate rocks which originated from deeper mantle sources. If the intermediate rocks were mainly mixtures of basic and acid magmas, they will then indicate a transitional (or a more complex) tectonic setting (Verma 2015b, 2015c; Verma et al., 2016a).

6. Conclusion

The new multi-dimensional discriminant-function based diagrams are the robust geochemical tools for deciphering tectonic setting of Precambrian igneous and meta-igneous rocks. These diagrams seem to work better once the several petrological explanations are taken into account together, such as crustal contamination, degree of mantle melting, and mantle vs crustal source characteristics.

In most cases, consistent results are obtained for the tectonic settings. The results are summarized as follows: (1) an arc setting for the Wadi Ghadir ophiolite, Egypt during the Neoproterozoic; (2) a collision setting for Zandspruit greenstone, Johannesburg dome, South Africa during the Mesoarchaean; (3) an arc or a transitional continental arc to collision tectonic setting for the Bulai Pluton, Central Limpopo Belt during the Neoarchaean; (4) an island arc setting for the Espungabera, Mozambique during the Mesoproterozoic; (5) an island arc setting for the Umkondo sills (Waterberg, Middelburg) Kalahari craton during the Mesoproterozoic;

(6) an island arc setting for the Iramba-Sekenke greenstone belt, central Tanzania during the Neoarchaean; (7) an arc or a transitional continental arc to collision tectonic setting for the Suguti area, northern Tanzania during the Neoarchaean; (8) a continental arc setting for the Chila, Axum area, northern Ethiopia during the Neoproterozoic; (9) a continental arc setting for the Bulbul-Kenticha domain, Negele area, northern Ethiopia during the Neoproterozoic; (10) a continental arc setting for the Werri area, northern Ethiopia during the Neoproterozoic; (11a) a continental arc setting for the Sangmelima region, Ntem complex, southern Cameroon during the Neoarchaean; (11b) a collision setting for the Ebolowa area, Ntem complex, southern Cameroon during the Neoarchaean; (12) a continental arc setting for the Birimian supergroup, southern Ghana during the Paleoproterozoic; and (13) an arc or a transitional continental arc to collision tectonic setting for the Katiola- Marabadiassa, Côte d'Ivoire during the Neoarchaean.

Acknowledgements

This work was partly supported by UNAM-PAPIIT project IN100816. I am extremely grateful to both reviewers Dr. Juan A. Moreno and Prof. Surendra P. Verma for numerous helpful comments, which enabled me to significantly improve my presentation.

References

Abd El–Rahman, Y., Polat, A., Dilek, Y., Fryer, B., El–Sharkawy, M., Sakran, S., 2009. Geochemistry and tectonic evolution of the Neoproterozoic Wadi Ghadir ophiolite, Eastern Desert, Egypt. Lithos 113, 158–178.

Agrawal, S. (1999), Geochemical discrimination diagrams: a simple way of replacing eye-fitted boundaries with probability based classifier surfaces. J. Geol. Soc. India, 54, 335–346.

Agrawal, S., Verma, S.P., 2007. Comment on "Tectonic classification of basalts with classification trees" by Pieter Vermeesch (2006): Geochim. Cosmochim. Acta 71, 3388–3390.

Aitchison, J., 1986. The Statistical Analysis of Compositional Data. Chapman and Hall, London, New York.

Anhaeusser, C.R., 2015. Metasomatized and hybrid rocks associated with a Palaeoarchaean layered ultramafic intrusion on the Johannesburg Dome, South Africa. J. Afr. Earth Sci. 102, 203–217.

Anum, S., Sakyi, P.A., Su, B.–X., Nude, P.M., Nyame, F., Asiedu, D., Kwayisi, D., 2015. Geochemistry and geochronology of granitoids in the Kibi–Asamankese area of the Kibi–Winneba volcanic belt, southern Ghana. J. Afr. Earth Sci. 102, 166–179.

Armstrong–Altrin JS., 2015. Evaluation of two multidimensional discrimination diagrams from beach and deep–sea sediments from the Gulf of Mexico and their application to Precambrian clastic sedimentary rocks. Int. Geol. Rev. 57, 1446–1461.

Armstrong–Altrin, J.S., Nagarajan, R., Lee, Y.I., Kasper–Zubillaga, J.J., Córdoba–Saldaña, L.P., 2014. Geochemistry of sands along the San Nicolás and San Carlos beaches, Gulf of California, Mexico: implications for provenance and tectonic setting. Turkish J. Earth Sci. 23, 533–558.

Bailie, R., Rajesh, H.M., Gutzmer, J., 2012. Bimodal volcanism at the western margin of the Kaapvaal Craton in the aftermath of collisional events during the Namaqua–Natal Orogeny: The Koras Group, South Africa: Precambr. Res. 200, 163–83.

Begg, G.C., Griffin, W.L., Natapov, L.M., O'Reilly, S.Y., Grand, S., O'Neill, C.J., Hronsky, J.M.A., Poudjom Djomani, Y., Swain, C.J., Deen, T., Bowden, P., 2009. The lithospheric architecture of Africa: seismic tomography, mantle petrology, and tectonic evolution. Geosphere 5, 23–50.

Bora, S., Kumar, S., 2015. Geochemistry of biotites and host granitoid plutons from Proterozoic Mahakoshal Belt, Central India Tectonic Zone: Implication on nature and tectonic setting of magmatism. Int. Geol. Rev. 57, 1686–1706.

Bouyoa, M.H., Penaye, J., Njel, U.O., Moussango, A.P.I., Sep, J.P.N., Nyama, B.A., Wassouo, W.J., Abaté, J.M.E., Yaya, F., Mahamat, A., Ye, H., Wu, F., 2016. Geochronological, geochemical and mineralogical constraints of emplacement depth of TTG suite from the Sinassi Batholith in the Central African Fold Belt (CAFB) of northern Cameroon: Implications for tectonomagmatic evolution. J. Afr. Earth Sci. 116, 9–41.

Bouyoa, M.H., Zhao, Y., Penaye, J., Zhang, S.H., Njel, U.O., 2015. Neoproterozoic subduction–related metavolcanic and metasedimentary rocks from the Rey Bouba Greenstone Belt of north–central Cameroon in the Central African Fold Belt: New insights into a continental arc geodynamic setting. Precambr. Res. 261, 40–53.

Buccianti, A., 2013. Is compositional data analysis a way to see beyond the illusion? Comput. Geosci. 50, 165–73.

Bullen, D.S., Hall, R.P., Hanson, R.E., 2012. Geochemistry and petrogenesis of mafic sills in the 1.1 Ga Umkondo large igneous province, southern Africa, Lithos 142–143, 116–129.

Cabanis, B., and Lecolle, M., 1989. Le diagramme La/10–Y/15–Nb/8: un outil pour la discrimination des séries volcaniques et la mise en évidence des processus de mélange et/ou de contamination crustale: Compte Rendu Academy Sciences Paris 309, 2023–29.

Doumbia, S., Pouclet, A., Kouamelan, A., Peucat, j.j., Vidal, M., Delor, C., 1998. Petrogenesis of juvenile–type Birimian (Paleoproterozoic) granitoids in Central Côte d'Ivoire, West Africa: geochemistry and geochronology. Precambr. Res.87, 33–63.

Egozcue, J.J., Pawlowsky–Glahn, V., Mateu–Figueras, G., and Barceló–Vidal, C., 2003. Isometric logratio transformations for compositional data analysis: Mathematical Geology 35, 279–300.

Ernst, W.G., 2009. Archaean plate tectonics, rise of Proterozoic supercontinentality and onset of regional, episodic stagnant–lid behavior. Gondwana Res. 15, 243–253.

Feybesse, J.L., Mil6si. J.P., 1994. The Archaean/Proterozoic contact zone in West Africa: a mountain belt of decollement thrusting and folding on a continental margin related to 2.1 Ga convergence of Archaean cratons? Precambr. Res. 69. 199 227.

Foley, S., 2008. A trace element perspective on Archaean crust formation and on the presence or absence of Archaean subduction. In: Book Condie, K.C., Pease, V. (Eds.). Geological Society of America Special Paper. Colorado, Boulder, pp. 31–50.

Furnes, H., Rosing, M., Dilek, Y., de Wit, M., 2009. Isua supracrustal belt (Greenland) da vestige of a 3.8 Ga suprasubduction zone ophiolite, and the implications for Archaean geology. Lithos 113, 115–132.

Goodwin, A.M., 1996. Principles of Precambrian Geology. Academic Press, London, p. 327.

Grebennikov, A.V., 2014. A–type granites and related rocks: Petrogenesis and classification. Russ.Geol. Geophys. 55, 1074–1086.

Grenholm, M., 2011. Petrology of Birimian Granitoids in Southern Ghana Petrography and Petrogenesis. unpublished bachelor thesis. Lund University, Sweden.

Hamilton, W.B., 2011. Plate tectonics began in Neoproterozoic time, and plumes from deep mantle have never operated. Lithos 123, 1–20.

Holzer, L., Frei, R., Barton, J.M., Kramers, J.D., 1998. Unraveling the record of successive high-grade events in the Central Zone of the Limpopo Belt using Pb single phase dating of metamorphic minerals. Precambr. Res. 87, 87–115.

Hu, P., Li, C., Li, J., Wang, M., Xie, C., Wu, Y., 2014. Zircon U–Pb–Hf isotopes and whole–rock geochemistry of gneissic granites from the Jitang complex in Leiwuqi area, eastern Tibet, China: Record of the closure of the Paleo–Tethys Ocean. Tectonophysics 623, 83–99

Janoušek, V., Moyen, J.F., Martin, H., Erban, V., Farrow, C., 2016. Classical Plots. Geochemical Modelling of Igneous Processes – Principles and Recipes in R Language Part of the series Springer Geochemistry pp 27–43.

Kaur, P., Chaudhria, N., Hofmann, A.W., 2015. New evidence for two sharp replacement fronts during albitisation of granitoids from northern Aravalli orogen, NW India. Int. Geol. Rev. 57, 1660–1685.

Laurent, O., Martin, H., Doucelance, R., Moyen, J–F., Paquette, J–L., 2011. Geochemistry and petrogenesis of high–K "sanukitoids" from the Bulai pluton, Central Limpopo Belt, South Africa: Implications for geodynamic changes at the Archaean–Proterozoic boundary. Lithos 123, 73–91.

Laurent, O., Doucelance, R., Martin, H., Moyen, J.F., 2013. Differentiation of the late-Archaean sanukitoid series and some implications for crustal growth: insights from geochemical modelling on the Bulai pluton, Central Limpopo Belt, South Africa. Precambrian Research 227, 186-203.

Ledru, P., Johan, V., Milesi, J.P., Teygey, M., 1994. Markers of the last stages of the Palaeoproterozoic collision: evidence for 2 Ga continent involving circum-South Atlantic provinces. Precambr. Res. 69, 169 191.

Manya, S., Maboko, M.A.H., 2008. Geochemistry and geochronology of Neoarchaean volcanic rocks of the Iramba–Sekenke greenstone belt, central Tanzania. Precambr. Res.163, 265–278,

Medlin, C. C., Jowitt, S. M., Cas, R. A. F., Smithies, R. H., Kirkland, C. L., Maas, R. A., Wingate, M. T. D., 2015. Petrogenesis of the A–type, Mesoproterozoic Intra–caldera Rheomorphic Kathleen Ignimbrite and Comagmatic Rowland Suite Intrusions, West Musgrave Province, Central Australia: Products of Extreme Fractional Crystallization in a Failed Rift Setting. J. Petrol. in press, doi: 10.1093/petrology/egv007.

Meschede, M., 1986. A method of discriminating between different types of mid–ocean ridge basalts and continental tholeiites with the Nb–Zr–Y diagram: Chem. Geol. 56, 207–18.

Moabi, N.G., Grantham, G.H., Roberts, J., le Roux, P., Matola, R., 2015. The geology and geochemistry of the Espungabera Formation of central Mozambique and its tectonic setting on the eastern margin of the Kalahari Craton. J. Afr. Earth Sci. 101, 96–112.

Mtoro, M., Maboko, M.A.H., Manya, S., 2009. Geochemistry and geochronology of the bimodal volcanic rocks of the Suguti area in the southern part of the Musoma–Mara Greenstone Belt, Northern Tanzania, Precambr. Res. 174, 241–257.

Offler, R., Fergusson, C.L., 2016. Proto–Pacific–margin source for the Ordovician turbidite submarine fan, Lachlan Orogen, southeast Australia: Geochemical constraints. Sediment. Geol. 334, 53–65.

Pandarinath, K., 2014a. Tectonomagmatic origin of Precambrian rocks of Mexico and Argentina inferred from multi–dimensional discriminant–function based discrimination diagrams. J. South Am. Earth Sci. 56, 468–484.

Pandarinath, K., 2014b. Testing of the recently developed tectonomagmatic discrimination diagrams from hydrothermally altered igneous rocks of 7 geothermal fields. Turkish J. Earth Sci. 23, 412–426.

Pandarinath, K., Verma, S.K., 2013. Application of four sets of tectonomagmatic discriminant function based diagrams to basic rocks from northwest Mexico. J. Iber. Geol. 39, 181–195.

Pawlowsky–Glahn, V., Egozcue, J.J., 2006. Compositional data and their analysis: an introduction. In: Buccianti, A., Mateu–Figueras, G., and Pawlowsky–Glahn, V., eds. Compositional data analysis in the Geosciences: from theory to practice: The Geological Society of London Special Publication 164, 1–10.

Pearce, J.A., 1982, Trace element characteristics of lavas from destructive plate boundaries. In: Thorpe, R.S., ed. Andesites: Chichester, John Wiley & Sons, p. 525–48.

Pearce, J.A., Cann, J.R., 1973. Tectonic setting of basic volcanic rocks determined using trace element analyses: Earth Planet. Sci. Lett. 19, 290–300.

Pearce, J.A., Gale, G.H., 1977. Identification of ore–deposition environment from trace–element geochemistry of associated igneous host rocks: Geological Society of London Special Publication 7, 14–24.

Pearce, J.A., Norry, M.J., 1979. Petrogenetic implications of Ti, Zr, Y, and Nb variations in volcanic rocks: Contrib. Mineral. Petrol. 69, 33–47.

Pearce, J.A., Harris, N.B.W., Tindle, A.G., 1984. Trace element discrimination diagrams for the tectonic interpretation of granitic rocks. J. Petrol. 25, 956–983.

Pease, V., Percival, J., Smithies, H., Stevens, G., Van Kranendonk, M., 2008. When did plate tectonics begin? Evidence from the orogenic record. In: Book Condie, K.C., Pease, V. (Eds.). Geological Society of America Special Paper. Colorado, Boulder, pp. 199–228.

Perri, F., Critelli, S., Dominici, R., Muto, F., Ponte, M., 2015. Sourceland controls and dispersal pathways of Holocene muds from boreholes of the Ionian Basin, Calabria, southern Italy. Geol. Mag. 152, 957–972.

Poujol, M., Anhaeusser, C.R., 2001. The Johannesburg Dome, South Africa: new single zircon U–Pb isotopic evidence for early Archaean granite–greenstone development within the central Kaapvaal Craton. Precambr. Res.108, 139–158.

Rogers, G., Saunders, A.D., 1989. Magnesian Andesites from Mexico, Chile and the Aleutian Islands: Implications for Magmatism Associated with Ridge–Trench Collisions. In: Crawford, A.J. (Ed.), Boninites and Related Rocks. Unwin Hyman, London, pp. 416–445.

Rossignol, C., Bourquin, S., Poujol, M., Hallot, E., Dabard, M–P., Nalpas, T., 2016. The volcaniclastic series from the luang prabang basin, Laos: A witness of a triassic magmatic arc? J. Asian Earth Sci. 160, 159–183.

Shang, C.K., Satir, M., Siebel, W., Nsifa, E.N., Taubald, H., Liégeois, J.P., Tchoua, F.M., 2004. TTG magmatism in the Congo craton; a view from major and trace element geochemistry, Rb–Sr and Sm–Nd systematics: case of the Sangmelima region, Ntem complex, southern Cameroon. J. Afr. Earth Sci.40, 61–79.

Shahzeidi, M., Moayyed, M., Murata, M., Yui, T-F., Arai, S., Chen, F., Pirnia, T., Ahmadian, J., 2016. Late Ediacaran crustal thickening in Iran: Geochemical and isotopic constraints from the ~550 Ma Mishu granitoids (northwest Iran). Int. Geol. Rev. http://dx.doi.org/10.1080/00206814.2016.1198728.

Shervais, J.W., 1982. Ti–V plots and the petrogenesis of modern and ophiolitic lavas: Earth Planet. Sci. Lett. 59, 101–18.

Shirey, S.B., Kamber, B.S., Whitehouse, M.J., Mueller, P.A., Basu, A.R., 2008. A review of the isotopic and trace element evidence for mantle and crustal processes in the Hadean and Archaean: Implications for the onset of plate tectonic subduction. In: Book Condie, K.C., Pease, V. (Eds.). Geological Society of America Special Paper. Colorado, Boulder, pp. 1–30.

Sifeta, K., Roser, B.P., Kimura, J.–I., 2005. Geochemistry, provenance, and tectonic setting of Neoproterozoic metavolcanic and metasedimentary units, Werri area, Northern Ethiopia. J. Afr. Earth Sci.41, 212–234.

Stern, R.J. (Ed.), 2008. Modern–style Plate Tectonics Began in Neoproterozoic Time: an Alternative Interpretation of Earth’s Tectonic History. Geological Society of America Special Paper. Colorado, Boulder.

Tadesse–Alemu, A., 1998. Geochemistry of Neoproterozoic granitoids from the Axum area, northern Ethiopia. J. Afr. Earth Sci. 27, 437–460.

Tadesse, T., Hoshino, M., Suzuki, K., Iizumi, S., 2000. Sm–Nd, Rb–Sr and Th–U–Pb zircon ages of syn- and post-tectonic granitoids from the Axum area of northern Ethiopia. J. Afr. Earth Sci. 30, 313–327.

Tchameni, R., Mezger, K., Nsifa, N.E., Pouclet, A., 2000. Neoarchaean crustal evolution in the Congo Craton: evidence from K rich granitoids of the Ntem Complex, southern Cameroon. J. Afr. Earth Sci.30, 133–147.

Torres Sánchez, S. A., Augustsson, C., Barboza Gudiño, J. R., Jenchen, U., Ramírez Fernández, J. A., Abratis, M., Scherstén, A., 2015. Magmatic source and metamorphic grade of metavolcanic rocks from the Granjeno Schist: was northeastern Mexico a part of Pangaea?. Geol. J. in press, DOI: 10.1002/gj.2702.

Torsvik T. H., Cocks L. R. M., 2011. The Formation and Evolution of Africa: A Synopsis of 3.8 Ga of Earth History, The Palaeozoic palaeogeography of central Gondwana, Geological Society, London, Special Publications, eds van Hinsbergen D. J. J., Buiter S. J. H., Torsvik T. H., Gaina C., Webb S. J. 357, pp 137–168.

Van Kranendonk, M.J., 2010. Two types of Archaean continental crust: plume and plate tectonics on early earth. Am. J. Sci. 310, 1187–1209.

Velasco–Tapia, F., 2014. Multivariate Analysis, Mass Balance Techniques, and Statistical Tests as Tools in Igneous Petrology: Application to the Sierra de las Cruces Volcanic Range (Mexican Volcanic Belt). Hindawi Publishing Corporation, The Scientific World Journal Volume, Article ID 793236, 32.

Velikoslavinskii, S.D., Krylov, D.P., 2015. Geodynamic classification of intermediate magmatic rocks based on geochemical data. Petrology 23, 413–420.

Verma, S.K., Oliveira, E.P., 2013. Application of multidimensional discrimination diagrams and probability calculations to Paleoproterozoic acid rocks from Brazilian cratons and provinces to infer tectonic settings: J. South Am. Earth Sci. 45, 117–146.

Verma, S.K., Oliveira, E.P., 2015. Tectonic setting of basic igneous and metaigneous rocks of Borborema Province, Brazil using multi–dimensional geochemical discrimination diagrams: J. South Am. Earth Sci. 58, 309–317.

Verma, S.K., Pandarinath, K., Verma, S.P., 2012. Statistical evaluation of tectonomagmatic discrimination diagrams for granitic rocks and proposal of new discriminant–function–based multi–dimensional diagrams for acid rocks. Int. Geol. Rev. 54, 325–347.

Verma, S.P., 2009. Continental rift setting for the central part of the Mexican Volcanic Belt: a statistical approach: Open Geology Journal 3, 8–29.

Verma, S.P., 2010. Statistical evaluation of bivariate, ternary and discriminant function tectonomagmatic discrimination diagrams. Turkish J. Earth Sci. 19, 185–238.

Verma, S.P., 2013. Application of 50 multi–dimensional discrimination diagrams and significance tests to decipher compositional similarities and differences between Hawaiian and Icelandic volcanism: Int. Geol. Rev. 55, 1553–72.

Verma, S.P., 2015a. Monte Carlo comparison of conventional ternary diagrams with new log-ratio bivariate diagrams and an example of tectonic discrimination: Geochem. J. 49, 393–412.

Verma, S.P., 2015b. Present state of knowledge and new geochemical constraints on the central part of the Mexican Volcanic Belt and comparison with the Central American Volcanic Arc in terms of near and far trench magmas. Turkish J. Earth Sci. 24, 399–460.

Verma, S.P., 2015c. Origin, evolution, and tectonic setting of the eastern part of the Mexican Volcanic Belt and comparison with the Central American Volcanic Arc from conventional multielement normalized and new multidimensional discrimination diagrams and discordancy and significance tests. Turkish J. Earth Sci. 24, 111–164.

Verma, S.P., and Agrawal, S., 2011. New tectonic discrimination diagrams for basic and ultrabasic volcanic rocks through log-transformed ratios of high field strength elements and implications for petrogenetic processes: Rev Mex Cienc Geol. 28, 24–44.

Verma, S.P., Rivera–Gómez, M.A., 2013. Computer programs for the classification and nomenclature of igneous rocks: Episodes 36, 115–24.

Verma, S.P., Verma, S.K., 2013. First 15 probability–based multi–dimensional discrimination diagrams for intermediate magmas and their robustness against post–emplacement compositional changes and petrogenetic processes: Turkish J. Earth Sci. 22, 931–95.

Verma, S.P., Guevara, M., and Agrawal, S., 2006. Discriminating four tectonic settings: five new geochemical diagrams for basic and ultrabasic volcanic rocks based on log-ratio transformation of major-element data: J. Earth. Syst. Sci. 115, 485–528.

Verma, S.P., Verma, S.K., Pandarinath, K., Rivera–Gómez, M.A., 2011. Evaluation of recent tectonomagmatic discrimination diagrams and their application to the origin of basic magmas in Southern Mexico and Central America. Pure Appl. Geophys. 168, 1501–1525.

Verma, S.P., Pandarinath, K., Verma, S.K., Agrawal, S., 2013. Fifteen new discriminant–function–based multi–dimensional robust diagrams for acid rocks and their application to Precambrian rocks. Lithos 168–169, 113–123.

Verma, S.P., Verma, S.K., Oliveira, E.P., 2015a. Application of 55 multi–dimensional tectonomagmatic discrimination diagrams to Precambrian belts. Int. Geol. Rev. 57, 1553–1572.

Verma, S.K., Oliveira, E.P., Verma, S.P., 2015b. Plate tectonic settings for Precambrian basic rocks from Brazil by multidimensional tectonomagmatic discrimination diagrams and their limitations. Int. Geol. Rev. 57, 1566–1581.

Verma, S.P., Pandarinath, K., Rivera–Gómez, M. A., 2016a. Evaluation of the ongoing rifting and subduction processes in the geochemistry of magmas from the western part of the Mexican Volcanic Belt. J. South Am. Earth Sci. 66, 125–148.

Verma, S.P., Cruz–Huicochea, R., Díaz–Gonzalez, L., Verma, S.K., 2016b. A new computer program TecDIA for multidimensional tectonic discrimination of intermediate and acid magmas and its application to the Bohemian Massif, Czech Republic. J. Geosci. 60, 203–218.

Wood, D.A., 1980. The application of a Th–Hf–Ta diagram to problems of tectonomagmatic classification and to establishing the nature of crustal contamination of basaltic lavas of the British Tertiary volcanic province: Earth Planet. Sci. Lett. 50, 11–30.

Yihunie, T, Adachi, M., Yamamoto, K., 2006. Geochemistry of the Neoproterozoic metabasic rocks from the Negele area, southern Ethiopia: Tectonomagmatic implications. J. Afr. Earth Sci. 44, 255–269.

Yildiz, A., Kibici, Y., Bağci, M., Dumlupunar, İ., Kocabaş, C., Aritan, A. E., 2015. Petrogenesis of the post–collisional Eocene volcanic rocks from the Central Sakarya Zone (Northwestern Anatolia, Turkey): Implications for source characteristics, magma evolution, and tectonic setting. Arab. J. Geosci. 8, 11239–11260.

Zhou, J–L., 2015. Nature of Cryogenian felsic igneous rocks in Madagascar reevaluated: A comment on "From passive margin to volcano–sedimentary forearc: The Tonian to Cryogenian evolution of the Anosyen Domain of southeastern Madagascar" by Boger et al. [Precambrian Res. 247 (2014) 159–186]. Precambr. Res. 262, 123–126.

Figure legends

Figure 1. Simplified geologic map of the Africa (modified after Begg et al., 2009). Cratons: West African Craton, Congo Craton, Tanzanian Craton and Kaapvaal Craton. Numbers refer to location of the studied basic, intermediate and acid igneous and meta-igneous rocks (see Table 1).

Figure 2. A set of major element based multidimensional diagrams (see the subscript "mint" in all these diagrams) for intermediate rocks of Verma and Verma (2013) for the discrimination of island-arc (IA), continental-arc (CA), within-plate (CR+OI), and collisional (Col) tectonic settings. The tectonic field boundary coordinates are proving below. **(a)** IA+CA–CR+OI–Col (1+2–3+4–5) diagram, the coordinates of the field boundaries are (0.42744, -8.0) and (-0.67554, 0.27663) for IA+CA–CR+OI, (8.0, 5.53331) and (-0.67554, 0.27663) for IA+CA–Col, and (-8.0, 4.73569) and (-0.67554, 0.27663) for CR+OI–Col **(b)** IA–CA–CR+OI (1–2–3+4) diagram, the coordinates of the field boundaries are (8.0, 0.76690) and (-0.63205, 0.08764) for IA–CA; (-1.50230, -8.0) and (-0.63205, 0.08764) for IA–CR+OI; and (-2.73408, 8.0) and (-0.63205, 0.08764) for CA–CR+OI **(c)** IA–CA–Col (1–2–5) diagram, the coordinates of the field boundaries are (8.0, -3.06676) and (-0.71170, 0.24138) for IA–CA; (-1.18110, 8.0) and (-0.71170, 0.24138) for IA–Col; and (-3.55140, −8.0) and (-0.71170, 0.24138) for CA–Col **(d)** IA–CR+OI–Col (1–3+4–5) diagram, the coordinates of the field boundaries are (0.66776, -8.0) and (-0.44102, 0.17933) for IA–CR+OI; (8.0, 6.27226) and (-0.44102, 0.17933) for IA–Col; and (-8.0, 4.24657) and (-0.44102, 0.17933) for CR+OI–Col **(e)** CA–CR+OI–Col (2–3+4–5) diagram, the coordinates of the field boundaries are (-3.42497, 8.0) and (-0.033967, -0.10997) for CA–CR+OI; (8.0, -0.16286) and (-

0.033967, -0.10997) for CA–Col; and (-4.17272, -8.0) and (-0.033967, -0.10997) for CR+OI–Col (for more detail, please see Verma and Verma, 2013).

Table 1
Synthesis of the compilation of rock samples used in the present study for applying discrimination diagrams (-- Case studies).

Test study		Approximate location		Number of Samples* (*Table no.* **for results**)			Age, Epoch (Ma)	Rock type	Original Author´s tectonic setting	Inferred tectonic setting from [B; I; A]*	Reference
Region	Sub-region	Long. (°)	Lat. (°)	**B**	**I**	**A**					
				m2, t2	m, mt, t	m, mt, t					
North Africa											
1. Wadi Ghadir ophiolite Egypt	1. Eastern Desert	34.9	24.8	34, 34	50, 50, 50	2, 2, 2	Neoproterozoic (746±19)	ophiolite	island arc to back-arc	[(IA-MOR); (IA-CA); IA]	Abd El-Rahman et al. (2009)
South Africa											
2. Zandspruit greenstone	2. Johannesburg Dome	-26.0	27.9	11, 10	13, 9, 0	9, 8, 0	Mesoarchaean (3114±2.3)	komatiites granitoids	---	[IA; Col; Col]	Anhaeusser (2015)
3. Bulai pluton	3. Central Limpopo Belt	-23.2	29.4	---	11, 11, 11	14, 14, 14	Neoarchaean (2610-2577)	granitoids	---	[---; Col; (CA-Col)]	Laurent et al. (2011)
4. Espungabera	4. Mozambique	-20.5	32.7	---	27, 27, 27	---	Mesoproterozoic (1109 ± 0.6)	volcanic rocks, basaltic andesite	volcanic arc/subduction	[---; IA; ---]	Moabi et al. (2015)
5. Umkondo sills	5. Kalahari craton	-24.0	28.0	5, 5	14, 14, 12	---	Mesoproterozoic (1100)	igneous and mafic rocks	subduction	[IA; IA; ---]	Bullen et al. (2012)
East Africa											
6. Iramba–Sekenke greenstone belt, central Tanzania	6. Tanzania Craton	34.5	-4.30	14, 5	10, 10, 10	---	Neoarchaean (2742±27)	volcanic rocks	volcanic arc	[IA; IA; ---]	Manya and Maboko, (2008)
7. Suguti area northern Tanzania	7. southern Musoma-Mara greenstone belt, Tanzania Craton	34.2	-2.10	20, 20	12, 12, 12	25, 25, 25	Neoarchaean (2755±1)	volcanic rocks	arc to MORB	[IA; IA; CA-Col)]	Mtoro et al. (2009)
8. Chila, northern Ethiopia	8. Axum area	38.5	14.1	---	10, 10, 0	41, 41, 0	Neoproterozoic (800)	granitoids	volcanic arc	[---; CA; CA]	Tadesse-Alemu (1998)
9. Bulbul-Kenticha domain, southern Ethiopia	9. Negele area	39.5	4.40	20, 0	10, 3, 0	---	Neoproterozoic (789)	metabasic rocks	island arc	[IA, CA; ---]	Yihunie et al. (2006)
10. Werri area, northern Ethiopia	10. Tsaliet and Tembien Groups	39.0	13.5	4, 4	18, 18, 12	---	Neoproterozoic (?)	metavolcanic rocks	volcanic arc or MORB	[(IA-MOR); CA; ---]	Sifeta et al. (2005)

(Continued)

Table 1. (continued)

Test study		Approximate location		Number of Samples* (*Table no.* **for results**)			Age, Epoch (Ma)	Rock type	Original Author´s tectonic setting	Inferred tectonic setting from Int.; acid	Reference
Region	Sub-region	Long. (°)	Lat. (°)	**B**	**I**	**A**					
				m2, t2	m, mt, t	m, mt, t					
North Africa											
West Africa											
11a. Sangmelima region, southern Cameroon	11a. Ntem complex, Congo craton	11.5	2.4	---	11, 11, 4	24, 20, 10	Neoarchaean (~2800-2900)	TTG	subduction	[---; CA; CA]	Shang et al. (2004)
11b. Ebolowa area, southern Cameroon	11b. Ntem complex, Congo craton	11.3	3.10	---	---	11, 9, 5	Neoarchaean (2687-2666)	granitoids	---	[---; ---; Col]	Tchameni et al. (2000)
12.Birimian supergroup, southern Ghana	12. west Africa craton	-0.31	6.10	10, 0	3, 3, 3	23, 23, 22	Paleoproterozoic (2232-2169)	Basalts, granitoids	subduction	[IA; CA; CA]	Grenholm (2011); Anum et al. (2015)
13. Katiola- Marabadiassa, Côte d'Ivoire	13. west Africa craton	-5.1	8.2	---	---	48, 13, 12	Paleoproterozoic (2123-2108)	granitoids	volcanic arc	[---; ---; (CA-Col)]	Doumbia et al. (1998)

*__B__−two sets of basic magma based diagrams (Verma et al., 2006; Verma and Agrawal, 2011); *__I__−three sets of intermediate magma based diagrams (Verma and Verma, 2013); *__A__-four sets of acid magma based diagrams (Verma et al., 2012; Verma et al., 2013); m2− second set of major element-based diagrams (Verma et al., 2006); t2− second set of trace element-based diagrams (Verma and Agrawal 2011); m− major elements; mt−(immobile) major and trace elements; t−(immobile) trace elements, for each set, respectively; --- no sample; Inferred tectonic setting: IA−Island Arc, CA−Continental Arc, CR+OI−within-plate; Col−Collision.

Table 2.
Application of multidimensional diagrams to Neoproterozoic (746±19 Ma) basic rocks of the Wadi Ghadir, Egypt (Abd El-Rahman et al., 2009).

Reference	Discrimination diagram §	Total no. of samples (%)	Predicted tectonic affinity and number of discriminated samples (%)				
			IAB	CRB+OIB	CRB	OIB	MORB
Verma et al. (2006); log-ratios of major elements (m2)	IAB-CRB-OIB-MORB	34 (100)	12 (35)	---	9 (27)	3 (9)	***10*** (29)
	IAB-CRB-OIB	34 (100)	13 (38)	---	11 (33)	10 (29)	---
	IAB-CRB+MORB	34 (100)	13 (38)	---	11 (33)	---	***10*** (29)
	IAB-OIB-MORB	34 (100)	14 (41)	---	---	4 (12)	***16*** (47)
	CRB-OIB-MORB	34 (100)	---	---	11 (33)	3 (9)	***20*** (58)
Synthesis of all five diagrams of Verma et al. (2006)		**170 (100)**	**52 (31)**	**---**	**42 (25)**	**20 (11)**	***56*** **(33)**
Verma and Agrawal (2011); log-ratios of immobile major and trace elements (t2)	IAB-CRB+OIB-MORB	34 (100)	8 (23)	2 (6)	---	---	***24*** (71)
	IAB-CRB-OIB	34 (100)	25 (73)	---	0 (0)	9 (27)	---
	IAB-CRB+MORB	34 (100)	8 (23)	---	2 (6)	---	***24*** (71)
	IAB-OIB-MORB	34 (100)	8 (23)	---	---	5 (15)	***21*** (62)
	CRB-OIB-MORB	34 (100)	---	---	0 (0)	3 (9)	***31*** (91)
Synthesis of all five diagrams of Verma and Agrawal (2011)		**170 (100)**	**49 (29)**	**2 (---)**	**2 (1)**	**19 (11.0)**	***100*** **(59.0)**

Notes: §The groups discriminated in discriminant-function-based multi-dimensional DF1–DF2 diagrams are as follows (B in the tectonic names stands for basic rocks): island arc (IA), continental arc (CA), continental rift (CR), ocean island (OI), and mid-ocean ridge (MOR); the numbers in parentheses '()' are the percentages of samples plotting in a given field: the correct discrimination (also called % success or percentage) can be seen in the column with italic boldface numbers. The final row gives a synthesis of results as the number of samples plotting in all five diagrams are reported in the column of total number of samples whereas the sum of samples plotting in a given tectonic field are reported in the respective tectonic field column.

Table 3.
Application of multidimensional diagrams to Neoproterozoic (746±19 Ma) intermediate rocks of the Wadi Ghadir, Egypt (Abd El-Rahman et al., 2009).

Magma type, Figure name	**Figure type**	**Total number of samples**	**Number of discriminated samples**				
			Arc				
			IA+CA [x ± s] [p_IA+CA] Θ	**IA [x ± s] [p_IA] Θ**	**CA [x ± s] [p_CA] Θ**	**CR+OI [x ± s] [p_CR+OI] Θ**	**Col [x ± s] [p_Col] Θ**
Intermediate; Verma and Verma (2013); log-ratios of all major elements	(IA+CA-CR+OI-Col)	50	28 [0.889±0.139] (0.4686-0.9999)	---	---	19 [0.904±0.141] (0.5455-0.9988)	3 [0.787±0.181] (0.6414-0.9893)
	(IA-CA-CR+OI)	50	---	9 [0.857±0.178] (0.5040-1.0000)	24 [0.766±0.145] (0.4592-0.9768)	17 [0.901±0.101] (0.6832-0.9982)	---
	(IA-CA-Col)	50	---	17 [0.822±0.145] (0.5304-1.0000)	27 [0.737±0.126] (0.5138-0.9484)	---	6 [0.650±0.198] (0.4661-0.9905)
	(IA-CR+OI-Col)	50	---	28 [0.885±0.130] (0.5175-1.0000)	---	19 [0.921±0.113] (0.6223-0.9993)	3 [0.735±0.271] (0.4506-0.9906)
	(CA-CR+OI-Col)	50	---	---	30 [0.898±0.108] (0.5362-0.9994)	18 [0.896±0.126] (0.6556-0.9992)	2 [0.776±0.235] (0.6099, 0.9420)
Diagrams based on log-ratios of major elements	***{Σn} {Σprob} [%prob]***	**250**	**{28} {24.8793} [---]**	**{54} {46.4785} [26.7%]**	**{81} {65.2412} [37.5%]**	**{73} {66.1291} [31.1%]**	**{14} {10.0204} [4.6%]**
Intermediate; Verma and Verma (2013); log-ratios of immobile major and trace elements	(IA+CA-CR+OI-Col)	50	25 [0.937±0.158] (0.4773-1.0000)	---	---	24 [0.846±0.201] (0.4263-0.9997)	1(0.5714)
	(IA-CA-CR+OI)	50	---	35 [0.767±0.184] (0.3768-0.9998)	7 [0.645±0.130] (0.5297-0.8931)	8 [0.855±0.168] (0.3768-0.9998)	---
	(IA-CA-Col)	50	---	29 [0.672±0.137] (0.4150-0.8710)	17 [0.648±0.152] (0.3898-0.8924)	---	4 [0.9193±0.0066] (0.9144-0.9288)
	(IA-CR+OI-Col)	50	---	25 [0.930±0.171] (0.4033-1.0000)	---	23 [0.872±0.177] (0.4745-0.9995)	2 [0.571±0.157] (0.4601, 0.6819)
	(CA-CR+OI-Col)	50	---	---	32 [0.916±0.154] (0.4850-1.0000)	18 [0.855±0.182] (0.4807-0.9994)	0 (0)
Diagrams based on log-ratios of major elements	***{Σn} {Σprob} [%prob]***	**250**	**{25} {23.4157} [---]**	**{89} {69.6001} [41.0%]**	**{56} {44.8509} [26.4%]**	**{73} {62.6004} [30.0%]**	**{7} {5.3907} [2.6%]**
Intermediate; Verma and Verma (2013); log-ratios of immobile trace elements	(IA+CA-CR+OI-Col)	50	40 [0.930±0.113] (0.5299-1.0000)	---	---	0 (0)	10 [0.763±0.162] (0.5117-0.9890)
	(IA-CA-CR+OI)	50	---	37 [0.857±0.130] (0.5384-0.9999)	6 [0.640±0.150] (0.4673-0.8397)	7 [0.703±0.222] (0.4140-0.9201)	---
	(IA-CA-Col)	50	---	37 [0.829±0.146] (0.4906-0.9998)	5 [0.516±0.085] (0.3790-0.5845)	---	8 [0.844±0.139] (0.6192-0.9586)
	(IA-CR+OI-Col)	50	---	40 [0.939±0.119] (0.4891-1.0000)	---	0 (0)	10 [0.792±0.134] (0.6043-0.9896)
	(CA-CR+OI-Col)	50	---	---	44 [0.912±0.136] (0.4438-1.0000)	0 (0)	6 [0.783±0.107] (0.6596-0.9363)
Diagrams based on log-ratios of immobile trace elements	***{Σn} {Σprob} [%prob]***	**250**	**{40} {37.2126} [---]**	**{114} {99.9457} [58.1%]**	**{55} {46.5704} [27.1%]**	**{7} {4.9199} [2.3%]**	**{34} {27.0006} [12.5%]**

IA−island arc; CA−continental arc; IA+CA–combined island and continental arcs, i.e., arc setting; CR−continental rift; OI−ocean island; CR+OI –combined continental rift and ocean island, i.e., within-plate (WP) setting; Col−collision; Θ the probability values for samples from a given locality are represented by (pIA+CA) – probability for the combined island and continental arc setting in the first diagram; [pIA] – probability for the island arc setting in the diagrams; [pCA] – probability for the continental arc setting in the diagrams; [pCR+OI] – probability for the combined continental rift and ocean island setting in all diagrams; [pCol] – probability for the collision setting in the diagrams; − mean ± 1SD (standard deviation) of the probability estimates for all samples discriminated in a given tectonic setting; these are reported in [], the values are rounded mostly following the indications put forth by Verma (2005); the final rows give a synthesis of results as {Σn} {Σprob} [%prob], where {Σn} is the total number of samples or data points plotting in all five diagrams is reported in the column of total number of samples, whereas the sum of samples plotting in a given tectonic field is reported in the respective tectonic field column; {Σprob} is the sum of probability values for all samples plotting in a given tectonic field is reported in the respective tectonic field column; and [%prob] is the total probability of a given tectonic setting expressed in percent after assigning the probability of IA + CA to IA and CA (using weighing factors explained in Verma and Verma, 2013; Verma et al. 2012, 2013).

Table 4.
Application of multidimensional diagrams to Neoproterozoic (746±19 Ma) acid rocks of the Wadi Ghadir, Egypt (Abd El-Rahman et al., 2009).

Magma type, **Figure name**	**Figure type**	**Total number of samples**	**Number of discriminated samples**				
			Arc				
			IA+CA [x ± s] **[p_IA+CA] Θ**	**IA [x ± s]** **[pIA] Θ**	**CA [x ± s]** **[pCA] Θ**	**CR+OI [x ± s]** **[pCR+OI] Θ**	**Col [x ± s]** **[pCol] Θ**
Acid; Verma et al. (2012); log-ratios of all major elements	(IA+CA–CR–Col)	2	2 [0.9999±0.0000] (1.0000, 1.0000)	---	---	0 (0)	0 (0)
	(IA–CA–CR)	2	---	2 [0.9999±0.0000] (1.0000, 1.0000)	0 (0)	0 (0)	---
	(IA–CA–Col)	2	---	2 [0.9999±0.0000] (1.0000, 1.0000)	0 (0)	---	0 (0)
	(IA–CR–Col)	2	---	2 [1.0000±0.0000] (1.0000, 1.0000)	---	0 (0)	0 (0)
	(CA–CR–Col)	2	---	---	2 [1.0000±0.0000] (1.0000, 1.0000)	0 (0)	0 (0)
Diagrams based on log-ratios of major elements	***{Σn} {Σprob}*** ***[%prob]***	**10**	**{2} {2.0000}** **[---]**	**{6} {6.0000}** **[75%]**	**{2} {2.0000}** **[25%]**	**{0} {0} [0%]**	**{0} {0} [0%]**
Acid; Verma et al. (2013); log-ratios of all major elements	(IA+CA-CR+OI-Col)	2	2 [0.9999±0.0000] (1.0000, 1.0000)	---	---	0 (0)	0 (0)
	(IA-CA-CR+OI)	2	---	2 [0.9999±0.0000] (1.0000, 1.0000)	0 (0)	0 (0)	---
	(IA-CA-Col)	2	---	2 [0.9999±0.00006] (0.9999, 1.0000)	0 (0)	---	0 (0)
	(IA-CR+OI-Col)	2	---	2 [1.0000±0.0000] (1.0000, 1.000)	---	0 (0)	0 (0)
	(CA-CR+OI-Col)	2	---	---	2 [1.0000±0.00000] (1.0000, 1.0000)	0 (0)	0 (0)
Diagrams based on log-ratios of major elements	***{Σn} {Σprob}*** ***[%prob]***	**10**	**{2} {2.0000}** **[---]**	**{6} {5.9999}** **[75%]**	**{2} {2.0000}** **[25%]**	**{0} {0} [0%]**	**{0} {0} [0%]**
Acid; Verma et al. (2013); log-ratios of immobile major and trace elements	(IA+CA-CR+OI-Col)	2	2 [0.9937±0.00401] (0.9909, 0.9965)	---	---	0 (0)	0 (0)
	(IA-CA-CR+OI)	2	---	2 [0.844±0.116] (0.7620, 0.9266)	0 (0)	0 (0)	---
	(IA-CA-Col)	2	---	2 [0.867±0.117] (0.7839, 0.9500)	0 (0)	---	0 (0)
	(IA-CR+OI-Col)	2	---	2 [0.9953±0.0051] (0.9917, 0.9989)	---	0 (0)	0 (0)
	(CA-CR+OI-Col)	2	---	---	2 [0.9945±0.00333] (0.9922, 0.9969)	0 (0)	0 (0)
Diagrams based on log-ratios of immobile major and trace elements	***{Σn} {Σprob}*** ***[%prob]***	**10**	**{2} {1.9874}** **[---]**	**{6} {5.4132}** **[73%]**	**{2} {1.9890}** **[27%]**	**{0} {0} [0%]**	**{0} {0} [0%]**
Acid; Verma et al. (2013); log-ratios of immobile trace elements	(IA+CA-CR+OI-Col)	2	2 [0.9863±0.00270] (0.9844, 0.9882)	---	---	0 (0)	0 (0)
	(IA-CA-CR+OI)	2	---	2 [0.9972±0.00246] (0.9955, 0.9990)	0 (0)	0 (0)	---
	(IA-CA-Col)	2	---	2 [0.99803±0.0008] (0.9975, 0.9986)	0 (0)	---	0 (0)
	(IA-CR+OI-Col)	2	---	2 [0.9999±0.0000] (1.0000, 1.0000)	---	0 (0)	0 (0)
	(CA-CR+OI-Col)	2	---	---	2 [0.9990±0.00016] (0.9989, 0.9991)	0 (0)	0 (0)
Diagrams based on log-ratios of immobile trace elements	***{Σn} {Σprob}*** ***[%prob]***	**10**	**{2} {1.9726}** **[---]**	**{6} {5.9905}** **[75%]**	**{2} {1.9980}** **[25%]**	**{0} {0} [0%]**	**{0} {0} [0%]**

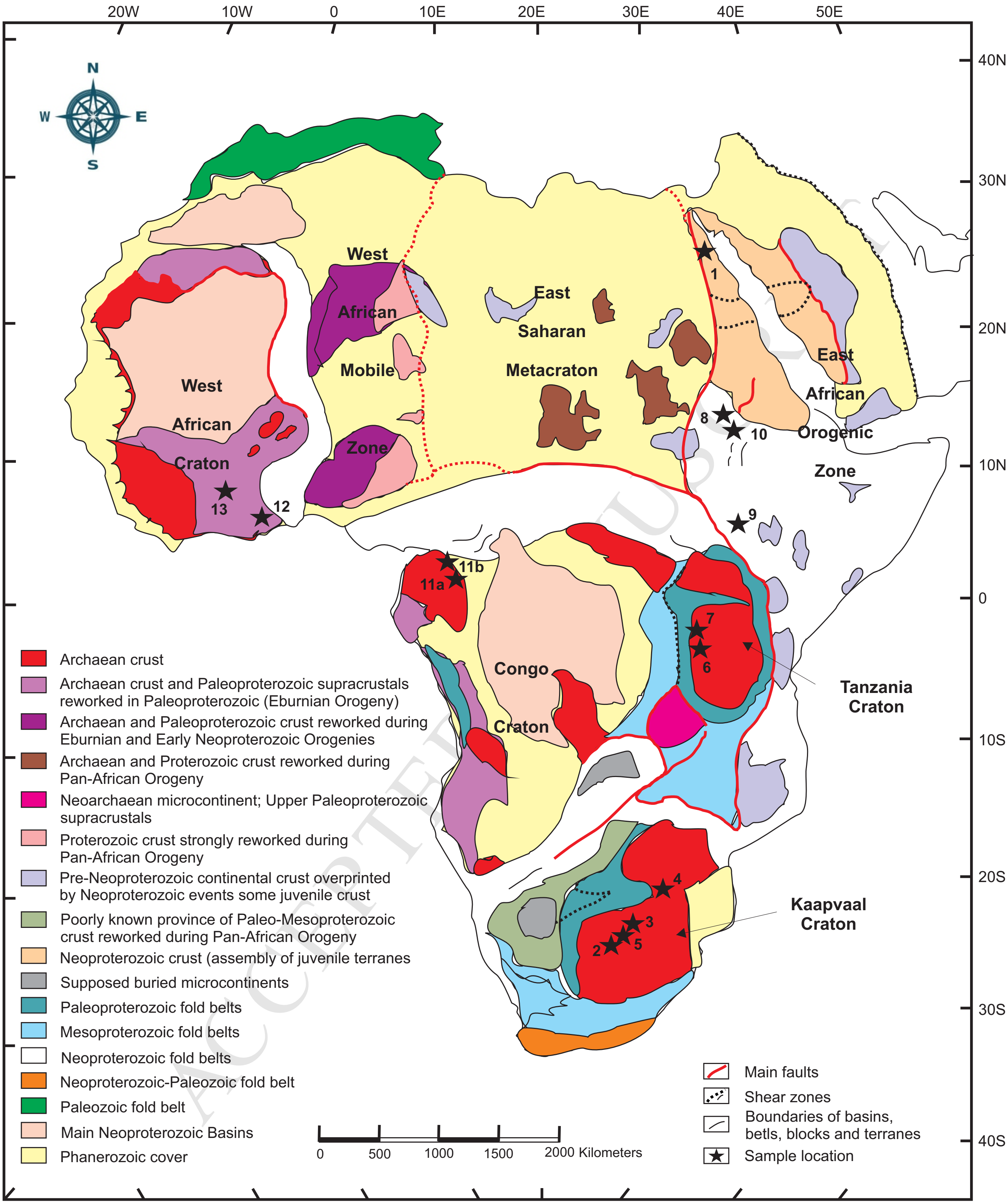

20W
10W
0
10E
20E
30E
40E
50E
40N
30N
20N
10N
0
10S
20S
30S
40S
N
W
E
S
West
African
Mobile
Zone
East
Saharan
Metacraton
West
African
Craton
East
African
Orogenic
Zone
Congo
Craton
Tanzania
Craton
Kaapvaal
Craton
1
2
3
4
5
6
7
8
9
10
11a
11b
12
13
Archaean crust
Archaean crust and Paleoproterozoic supracrustals reworked in Paleoproterozoic (Eburnian Orogeny)
Archaean and Paleoproterozoic crust reworked during Eburnian and Early Neoproterozoic Orogenies
Archaean and Proterozoic crust reworked during Pan-African Orogeny
Neoarchaean microcontinent; Upper Paleoproterozoic supracrustals
Proterozoic crust strongly reworked during Pan-African Orogeny
Pre-Neoproterozoic continental crust overprinted by Neoproterozoic events some juvenile crust
Poorly known province of Paleo-Mesoproterozoic crust reworked during Pan-African Orogeny
Neoproterozoic crust (assembly of juvenile terranes
Supposed buried microcontinents
Paleoproterozoic fold belts
Mesoproterozoic fold belts
Neoproterozoic fold belts
Neoproterozoic-Paleozoic fold belt
Paleozoic fold belt
Main Neoproterozoic Basins
Phanerozoic cover
0
500
1000
1500
2000 Kilometers
Main faults
Shear zones
Boundaries of basins, betls, blocks and terranes
Sample location

Figure 1

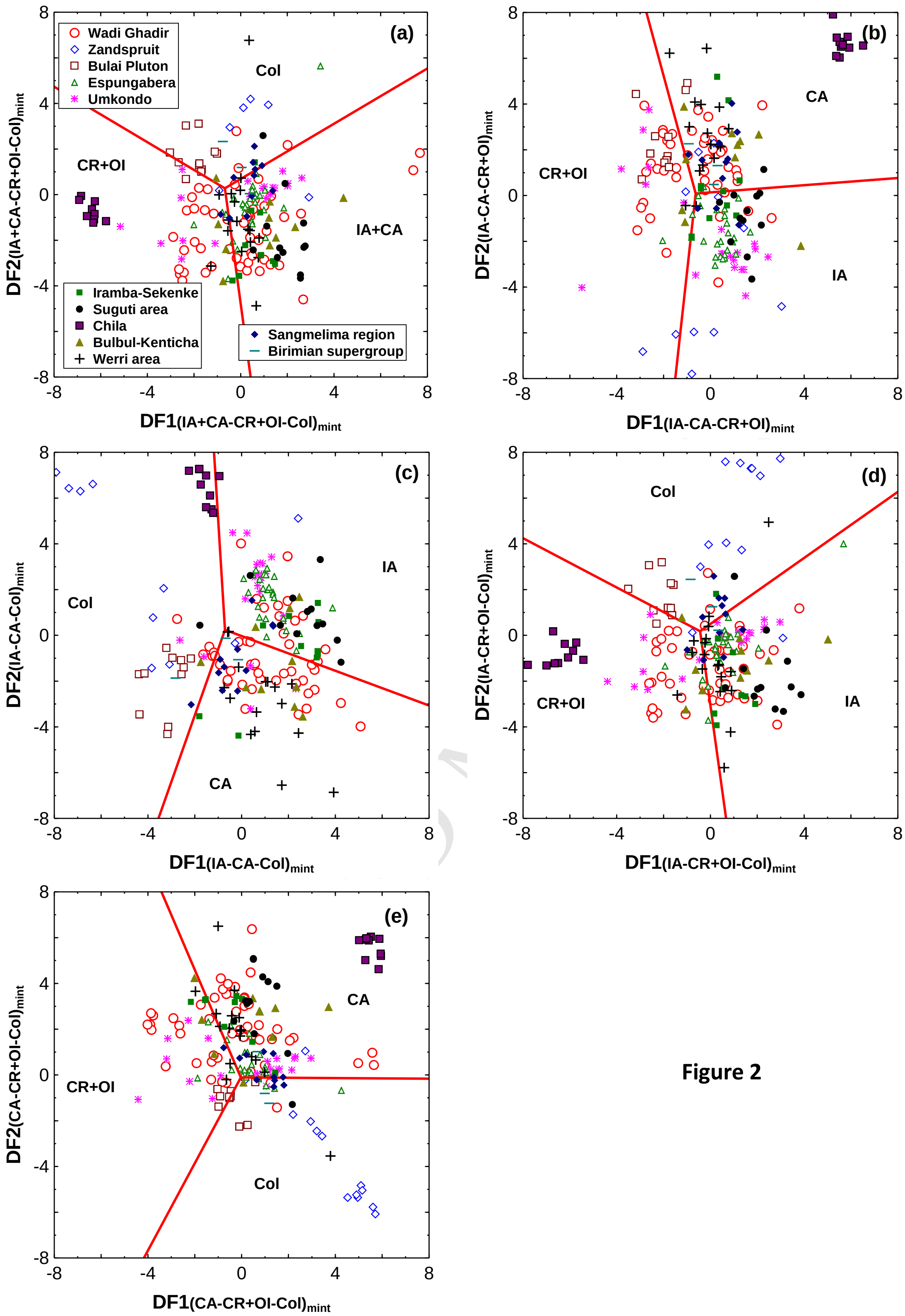

(a)
(b)
(c)
(d)
(e)
Wadi Ghadir
Zandspruit
Bulai Pluton
Espungabera
Umkondo
Iramba-Sekenke
Suguti area
Chila
Bulbul-Kenticha
Werri area
Sangmelima region
Birimian supergroup
Col
CR+OI
IA+CA
CA
IA
DF1(IA+CA-CR+OI-Col)mint
DF2(IA+CA-CR+OI-Col)mint
DF1(IA-CA-CR+OI)mint
DF2(IA-CA-CR+OI)mint
DF1(IA-CA-Col)mint
DF2(IA-CA-Col)mint
DF1(IA-CR+OI-Col)mint
DF2(IA-CR+OI-Col)mint
DF1(CA-CR+OI-Col)mint
DF2(CA-CR+OI-Col)mint

Figure 2

Nine sets of new multi-dimensional geochemical discrimination diagrams (two sets of major elements, immobile trace elements by Verma et al., 2006; Verma and Agrawal, 2011 for basic rocks; three sets of major elements, major-trace elements and immobile trace elements by Verma and Verma 2013 for intermediate rocks; two sets of major elements, one major-trace elements and one immobile trace elements based diagrams by Verma et al., 2012, 2013 for acid rocks) were used to identify plate tectonic setting of Precambrian rocks from Africa.